^{129}Xe-Cs (D$_{1}$,D$_{2}$) versus ^{129}Xe-Rb (D$_{1}$) spin-exchange optical pumping at high xenon densities using high-power laser diode arrays

Nicholas Whiting, Neil A. Eschmann, Boyd M. Goodson, and Michael J. Barlow

^{129}Xe/Cs (D$_1$, D$_2$) Versus ^{129}Xe/Rb (D$_1$) Spin-Exchange Optical Pumping at High Xenon Densities Using High-Power Laser Diode Arrays

Nicholas Whiting,[*] Neil A. Eschmann,[†] and Boyd M. Goodson[‡]

Department of Chemistry and Biochemistry,

Southern Illinois University, Carbondale IL 62901

Michael J. Barlow

Sir Peter Mansfield Magnetic Resonance Centre,

University of Nottingham, Nottingham, NG7 2RD, UK

Abstract

We investigate ^{129}Xe/Cs (D$_1$ & D$_2$) spin exchange optical pumping (SEOP) at high Xe densities ($\sim$0.12-2.44 amagat) using newly available high-power ($>$40 W) laser diode arrays, and compare with ^{129}Xe/Rb D$_1$ SEOP under similar conditions. At elevated Xe densities, the spin-exchange rate (per alkali metal atom, γ') for Cs/^{129}Xe is $\sim$1.5-fold greater than that for Rb/^{129}Xe. Higher spin-exchange rates and lower ^{129}Xe spin-destruction rates for Cs/^{129}Xe versus Rb/^{129}Xe contribute to $\sim$2-fold improvement in ^{129}Xe nuclear spin polarization measured at 9.4 T—with the largest gains observed at the highest Xe densities.

[*]Current address: SPMMRC, U. Nottingham, Nottingham, NG7 2RD, UK

[†]Current address: Chem. Dept., U.C. Santa Barbara, CA

[‡]Electronic address: `bgoodson@chem.siu.edu`

I. INTRODUCTION

The high nuclear spin polarization of hyperpolarized (HP) noble gases (e.g. ^{3}He and ^{129}Xe) has been exploited for a wide range of applications, from magnetic resonance spectroscopy and imaging [1] to fundamental physics experiments [2]. While ^{3}He has a larger magnetic moment and a higher diffusivity (useful for probing lung pathologies [3]), ^{129}Xe offers greater chemical shift sensitivity and proclivity for interacting with molecular and materials surfaces. Moreover, ^{129}Xe is relatively abundant; thus, the world-wide ^{3}He shortage [4] provides further urgency for the development of improved HP^{129}Xe approaches.

HP^{129}Xe is typically produced via spin-exchange optical pumping (SEOP) with an alkali metal vapor [5, 6]. Rubidium has been the alkali metal of choice for HP gas preparation because of its large spin-exchange cross sections [5], relatively high vapor pressures, and the abundance of inexpensive, high-power light sources (i.e. laser diode arrays, LDAs) that emit at its D-line absorption wavelengths [7]. Nevertheless, there may be advantages to using *cesium* for SEOP: for example, the Cs/^{129}Xe binary spin-exchange cross section has been measured to be ~1.9 times greater than that of Rb/^{129}Xe [8], while the Cs/^{129}Xe collisional spin-destruction cross section (which quantifies the loss of electron spin polarization with increasing Xe density) may be only half that of Rb/^{129}Xe [9, 10]. Additionally, Cs has even higher vapor pressures[11], lower-energy D lines (giving more photons per Watt of light) [12], and greater D-line spacing [13]. Yet despite these anticipated advantages and considerable effort (e.g. Refs. [12, 14, 15]), improved results with Cs have yet to be realized and Cs/^{129}Xe SEOP is still not widely practiced. Indeed, the development of Cs/^{129}Xe SEOP has been hindered by the lack of available high-power light sources that emit at the Cs D lines (equivalent to those available for Rb [8]), preventing the proper exploration of the SEOP parameter space [16]—and hence, limiting the xenon polarization that can be achieved.

In this work, we investigate ^{129}Xe/Cs SEOP using newly available high-power LDAs that emit at the Cs D$_1$ or D$_2$ lines, and compare with ^{129}Xe/Rb D$_1$ SEOP performed under similar conditions. At elevated Xe densities (~0.61-2.44 amagat [17], or 100-2000 Torr), the per-atom spin-exchange rate for Cs/^{129}Xe is ~1.5-fold greater than that for Rb/^{129}Xe—in good agreement with previous measurements [8, 18]. Higher spin-exchange rates and lower ^{129}Xe spin-destruction rates for Cs/^{129}Xe versus Rb/^{129}Xe contribute to a ~2-fold average

improvement in ^{129}Xe spin polarization (P_{Xe}) measured at 9.4 T—with the largest gains observed at the highest Xe densities.

II. METHODS

Aspects of our SEOP apparatus have been described previously [16, 19]. Briefly, "batch-mode" SEOP was performed using Surfasil-coated Rosen [20] cells (Pyrex, 75 cc, 1" o.d. inner cell/cylinder, 2" o.d. outer cylinder); in the Rosen cell design, the inner cell volume contains the alkali metal and the gases under study, whereas the outer volume is used as a forced-air oven to heat the contents of the inner cell. Each Rosen cell was loaded with either Rb or Cs and variable Xe/N$_2$ mixtures [21], and illuminated with broadband AlGaAs LDAs (QPC, Sylmar, CA) tuned to the Cs (D$_1$=894.3 nm or D$_2$=852.1 nm) or Rb (D$_1$=794.8 nm) lines. Nominal laser conditions (Fig. 1): Cs D$_1$: ∼46 W, $\Delta\lambda_{fwhm}$=2.9 nm; Cs D$_2$: ∼40 W, $\Delta\lambda_{fwhm}$=1.9 nm; Rb D$_1$: ∼53 W, $\Delta\lambda_{fwhm}$=2.1 nm. The LDAs were mounted to water-cooled plates and driven with Xantrex power supplies (6 V, 110 Amp for Cs lasers, 12 V, 70 Amp for Rb laser). The laser output is fiber-coupled into a home-built monocular circular polarizer box (with broadband near-IR optics comprising a collimating lens, a corner-cube, a rotatable quarter-wave plate, and a beam dump). The short (30 cm) polarization-preserving fiber retains most of the linear polarization of the emitted laser light, resulting in an efficient (∼90/10) straight/angled beam ratio (the "angled" beam is directed into the beam dump, whereas the "straight" beam is delivered to the cell; this design mitigates the issue of off-axis pumping [22] which may confound studies utilizing binocular optics for circularly polarizing the LDA output). A 2" mirror mounted behind the cell retroreflects transmitted laser light back into the cell; each laser's transmitted spectral profile is monitored by a high-resolution near-IR spectrometer (Ocean Optics) via an optical fiber probe mounted just behind the mirror. The cell resides in a Helmholtz coil (HC) pair (22" i.d., ∼32 G) and is supported and positioned with custom (non-magnetic) PTFE mounts and Garolite posts on translation stages.

^{129}Xe polarization dynamics were monitored *in situ* using a low-field NMR spectrometer (Magritek Aurora; nominal ^{129}Xe NMR frequency: 37.5 kHz) and homebuilt detection coil (with noise-suppressing counter-wound bucking coil [23]). Low-field NMR signals were acquired with a single rf pulse following re-zeroing P_{Xe} (via the application of ∼300-500

'crusher' pulses) and subsequent laser illumination of the cell for a variable time. For high-field NMR measurements, hyperpolarized xenon was collected following SEOP at optimal temperatures (T_{OPT} [24]) by expanding the contents of the cell into a pre-evacuated volume that includes a stopcock-sealed NMR tube. ^{129}Xe NMR spectra were recorded via the application of a single (1 μs, 6.7° tipping angle) rf pulse following transfer to 9.4 T using a Varian Inova spectrometer. The absolute P_{Xe} value was determined via comparison with a thermally polarized ^{129}Xe NMR signal from the same sample (obtained following careful addition of sufficient O_2 gas to reduce the ^{129}Xe T_1 (to a few s) to permit signal averaging).

III.   RESULTS AND DISCUSSION

A. ^{129}Xe/Cs SEOP: D_1 vs. D_2 Excitation.

Examples of high-field HP^{129}Xe NMR spectra obtained following ^{129}Xe/Cs D_2 or D_1 SEOP are shown in Fig. 2. Unlike with D_1 excitation, D_2 pumping drives population from *both* ground-state sublevels (with repopulation via relaxation at effectively equal rates because of collisional mixing of the excited states [25]). However, the ground-state sublevels are *de*-populated at a 1:3 ratio [25, 26]; thus, the alkali metal electron spin polarization ($|P_{AM}|$) can theoretically approach 0.5 for D_2 optical pumping (*cf.* a limit of $|P_{AM}|$=1 for D_1 OP). Thus, significant ^{129}Xe polarization can still be achieved using Cs SEOP at the D_2 line [14]. Greater light absorption at the D_2 line caused by the ∼2-fold higher oscillator strength [27] gives rise to lower optimal cell temperature (T_{OPT}) values [24] when switching from D_1 to D_2 SEOP. Because of the 1:3 depopulation ratio, performing SEOP at the D_2 versus the D_1 Cs line—but with the same light helicity—polarizes the ^{129}Xe in the opposite direction (Fig. 2). This effect also illustrates the source of concern regarding inadvertent D_2 pumping when performing *rubidium* D_1 SEOP with broadband sources [10, 13, 28], as any light absorbed at the wing of the D_2 line would tend to depolarize the noble gas.

B. Low-Field Measurements of ^{129}Xe/Cs & ^{129}Xe/Rb Spin-Exchange and ^{129}Xe Spin-Destruction.

The availability of LDAs with emission at the Cs (D_1 & D_2) and Rb (D_1) lines allows direct comparison of SEOP phenomena under otherwise similar conditions. Low-field *in situ* ^{129}Xe NMR build-up curves were obtained for various cell temperatures (T_{cell}) and Xe densities (e.g. Fig. 3a), and were fit to an exponential [29]:

$$S(t) = S_\infty[1 - \exp(-\Gamma t)], \tag{1}$$

where the time constant is given by: $\Gamma = \gamma_{SE} + \Gamma_{Xe}$, γ_{SE} is the spin-exchange rate, Γ_{Xe} is the ^{129}Xe nuclear spin-destruction rate ($=1/T_1^{Xe}$), and S_∞ is the steady-state low-field ^{129}Xe NMR signal, given by:

$$S_\infty \propto P_{Xe} = \langle P_{AM} \rangle \frac{\gamma_{SE}}{\Gamma}. \tag{2}$$

A linear fit of Γ values plotted versus the alkali metal density ([AM]) should provide measures of the per-atom spin-exchange rate ($\gamma' = \gamma_{SE}/[AM]$) and the ^{129}Xe spin-destruction rate (Γ_{Xe}) from the slope and y-intercept, respectively [29] (Figs. 3(b,c)). Here, alkali metal densities are estimated from vapor-pressure curves [27, 30].

As discussed below, a significant dependence upon the Xe density ([Xe]) was not expected under our conditions—as confirmed for Rb (Fig. 3b; see also Fig. 4). Indeed, the Rb data can be fit in aggregate to obtain overall 'average' values of $\gamma' = 1.67 \pm 0.06 \times 10^{-15}$ cm^3/s and $\Gamma_{Xe} = 3.4 \pm 0.2 \times 10^{-3}$ s^{-1}. The Cs data exhibit not only a steeper dependence upon the alkali metal density, but also a larger spread resulting from an apparent dependence of spin-exchange rate upon the Xe density (^{129}Xe spin-destruction does not show a clear [Xe] dependence). In part because ^{129}Xe spin-destruction is much slower for Cs than Rb, fitting the Cs data in aggregate requires fixing Γ_{Xe} (here set to $4 \pm 3 \times 10^{-4}$ s^{-1}, the average obtained from separate fits for each Xe density)—yielding $\gamma' = 2.6 \pm 0.1 \times 10^{-15}$ cm^3/s ($\sim$1.5-fold greater than for Rb). Plots of the per-atom spin-exchange rate versus Xe partial pressure for Cs D_1, Cs D_2, and Rb D_1 SEOP are shown in Fig. 4. The dependence for the Rb data is relatively flat; however, both sets of Cs data exhibit per-atom spin-exchange rates similar to those of Rb at low Xe partial pressures, but significantly greater values at higher Xe pressures ($\geq$500 Torr)—again, giving an average ratio of $\gamma'_{CsXe}/\gamma'_{RbXe} \sim 1.5$ over this range [31].

This ratio is in good agreement with recent measurements of Cs/^{129}Xe and Rb/^{129}Xe

5

spin exchange performed under internally comparable conditions [8, 18], but a more detailed interpretation is complicated by several factors. For example, the per-atom spin-exchange rates (γ') in Fig. 4, while in the range of previous measurements [5, 8, 18, 29, 32, 33], are higher than recently reported values. The alkali metal densities in Fig. 4 were calculated from oven air temperatures [27, 29, 30]; however, values predicted from empirical curves can deviate systematically from direct measurements [8, 18, 22]. In previous studies using Rosen cells [16], we found a 13-15 °C difference between the temperatures of the oven air exhaust and the (hotter) outer wall of the cell during SEOP. Accounting for this difference reduces the per-atom spin-exchange rates by $\sim$2.3-fold (more in line with expectations)—but importantly has little effect on the $\gamma'_{CsXe}/\gamma'_{RbXe}$ ratio.

Next, the per-atom spin-exchange rate is often partitioned as a sum of the binary spin-exchange cross-section ($\langle\sigma\nu\rangle$, from two-body alkali/^{129}Xe collisions) and a three-body term given by $\gamma_M\zeta([\text{Xe}]+b[\text{N}_2])^{-1}$, where γ_M is the molecular spin-exchange rate, b is a factor that accounts for the presence of both Xe and N$_2$ in the cell (and their capacities to modulate the formation and breakup of transient alkali/^{129}Xe van der Waals complexes), and ζ is a parameter determined by the relative abundances and nuclear spins of the involved alkali metal isotopes (as well as by P_{AM} and the molecular lifetime) [5, 18, 29, 34, 35]. While the 3-body term is expected to dominate at low total pressures ($<$100s of Torr), at sufficiently high pressures the molecular lifetimes should ultimately become short enough to reduce the spin-exchange rate to the ([Xe]-independent) 2-body limit [8]. Happer and co-workers used high pressures (and high magnetic fields) to suppress the 3-body contribution and obtain measurements of $\langle\sigma\nu\rangle_{CsXe}$=2.81$\times10^{-16}$ cm^3/s and $\langle\sigma\nu\rangle_{RbXe}$=1.75$\times10^{-16}$ cm^3/s at 9.4 T (giving $\gamma'_{CsXe}/\gamma'_{RbXe}\sim$1.6) [8]. When extrapolated to low field, these values translate to 4.1$\times10^{-16}$ and 2.2$\times10^{-16}$ cm^3/s, respectively (giving a ratio of $\sim$1.9). Hughes and co-workers performed experiments at low field and lower gas densities ($\sim$0.2-0.7 amg) to measure both 2-body and 3-body spin-exchange contributions [18]; they reported per-atom spin-exchange rates of $\sim$1.9-5.4$\times10^{-15}$ and $\sim$1.5-3.2$\times10^{-15}$ cm^3/s for Cs/^{129}Xe and Rb/^{129}Xe, respectively, corresponding to a range of $\gamma'_{CsXe}/\gamma'_{RbXe}$ ratios of $\sim$1.2-1.7—again in good agreement with our results. However, the partitioning of their spin-exchange rates is surprising, with a large $\langle\sigma\nu\rangle_{RbXe}$ value ($\sim$1.0$\times10^{-15}$ cm^3/s) and a $>$10-fold *smaller* $\langle\sigma\nu\rangle_{CsXe}$ value ($\sim$9.4$\times10^{-17}$ cm^3/s), that—when combined with relatively large values for b_{CsXe} and γ_M^{CsXe} of 0.97 and 4.92$\times10^5$ s^{-1} (*cf.* 0.275 [29] and 1.02$\times10^5$ s^{-1} for Rb/^{129}Xe)—translates

to a disproportionately large contribution from the 3-body term [18]. Thus, extrapolation to our (higher-pressure) conditions would predict the Cs/^{129}Xe spin-exchange rate to be >2-fold *smaller* than that of Rb/^{129}Xe. Our γ'_{CsXe} values are sensitive to Xe density, but with the opposite trend. Given potential flaws in relaxation models involving transient van der Waals complexes [18, 36], extrapolation of their results to our regime may be problematic. Measurements of higher per-atom spin-exchange rates with increasing Xe density have been reported previously [16, 32], but cannot be readily understood in terms of the current model [5, 29]. In any case, for spin-exchange measurements obtained under comparable conditions, the $\gamma'_{CsXe}/\gamma'_{RbXe}$ ratio is arguably the most useful quantity for evaluating the utility of Cs/^{129}Xe SEOP because it avoids the above complications (as well as many systematic errors). While obtained in different regimes, the data from the present work and Refs. [8, 18] indicate generally higher per-atom spin-exchange rates for Cs/^{129}Xe compared to Rb/^{129}Xe.

We also observed slower ^{129}Xe spin relaxation (Γ_{Xe}) in Cs- versus Rb-loaded cells. This effect is reminiscent of previous ^{3}He experiments [37] that found that Cs provided the longest ^{3}He T_1's of all the coatings studied—several-fold longer than similar Rb-coated cells—and suggests that Cs coatings may be more effective at partitioning ^{129}Xe from paramagnetic centers near the cell's surfaces.

C. High-Field Measurements of P_{Xe}.

Finally, the availability of LDAs that emit at the Cs and Rb D_1 lines—but with similar (high, $\geq$40 W) output powers and linewidths—permits side-by-side comparison of Xe polarization under conditions relevant for enhanced NMR and MRI. A series of batch-mode SEOP runs were performed using Cs or Rb cells with variable Xe partial pressures; P_{Xe} values were measured via NMR following gas collection and transfer to high field (Fig. 5). ^{129}Xe polarization values achieved via Cs/^{129}Xe SEOP exceeded those obtained via Rb/^{129}Xe SEOP by an average of $\sim$2-fold—with the greatest improvements observed at the highest Xe densities (consistent with the $\gamma'_{CsXe}/\gamma'_{RbXe}$ trend in Fig. 4). The P_{Xe} values in Fig. 5 are plotted along side estimates for the cell-averaged alkali metal electron spin polarization ($\langle P_{AM} \rangle$; see Caption). In addition to faster spin exchange, slower ^{129}Xe spin relaxation should cause P_{Xe} to track P_{AM} more closely for Cs (giving an edge over Rb even at the lowest Xe densities studied). The contributions from *alkali metal* spin-destruction (Γ_{SD})

cannot be quantified without direct measurements of P_{AM}. However, given the similarities of the Cs/^{129}Xe and Rb/^{129}Xe OP conditions, the steeper fall-off in estimated $\langle P_{Rb} \rangle$ values with increasing Xe density would be consistent with predictions that $\Gamma_{SD}^{Rb} \gtrsim \Gamma_{SD}^{Cs}$ [9, 10] (providing another potential advantage for using Cs for polarizing Xe—particularly at high Xe densities).

IV. SUMMARY

We have utilized newly available high-power broadband LDAs to investigate and compare ^{129}Xe/Cs and ^{129}Xe/Rb SEOP for HP^{129}Xe generation. Higher spin-exchange rates and lower ^{129}Xe spin-destruction rates for Cs/^{129}Xe versus Rb/^{129}Xe contributed to a ~2-fold average improvement in P_{Xe}—with the largest gains observed at the highest Xe densities. We anticipate further gains with the advent of high-power *line-narrowed* LDAs [16, 38] at Cs wavelengths. While the present results concern batch-mode ^{129}Xe SEOP, we expect they will also be relevant to other noble gas isotopes [39] and experimental configurations [6], and open a door to novel studies of alternate hybrid (e.g. Cs/Rb and Cs/K) cells. Thus, these results could have significant impact on a wide range of spectroscopic, biomedical imaging, and fundamental physics applications utilizing HP gases.

V. ACKNOWLEDGMENTS

[1] B.M. Goodson, J. Magn. Reson. **155**, 157 (2002); A. Bifone, and A. Cherubini, Prog. Nucl. Magn. Reson. Spectrosc. **42**, 1 (2003).

[2] J.L. Friar, et al., Phys. Rev. C **42**, 2310 (1990); E124 Collaboration, P. Anthony et al., Phys. Rev. Lett. **71**, 959 (1993); M.V. Romalis, and M.P. Ledbetter, Phys. Rev. Lett. **87**, 067601 (2001).

[3] D.A. Yablonskiy *et al.*, J. Appl. Physiol. **107**, 8750 (2009).

[4] W.P. Halperin, Testimony to The House Committee on Science & Technology, Washington, D.C., (2010).

[5] W. Happer et al., Phys. Rev. A **29**, 3092 (1984); X. Zeng et al., Phys. Rev. A **31**, 260 (1985); T. Walker, and W. Happer, Rev. Mod. Phys. **69**, 629 (1997).

[6] B. Driehuys, et al., Appl. Phys. Lett. **69**, 1668 (1996); I.C. Ruset, S. Ketel, F.W. Hersman, Phys. Rev. Lett. **96** 053002 (2006).

[7] M.E. Wagshul, and T.E. Chupp, Phys. Rev. A **40**, 4447 (1989).

[8] Y.-Y. Jau, N.N. Kuzma, and W. Happer, Phys. Rev. A **66**, 052710 (2002); ibid. **67**, 022720 (2003); ibid. **69** 061401 (2004).

[9] T.G. Walker, Phys. Rev. A **40**, 4959 (1989); I.A. Nelson, and T.G. Walker, Phys. Rev. A **65**, 012712 (2001).

[10] A.H. Couture, T. B. Clegg, and B. Driehuys, J. Appl. Phys. **104** 094912 (2008).

[11] The greater ease of vaporizing cesium at lower temperatures may be favorable for technical reasons [12]: For example, elevated cell temperatures can reduce the stability of organic coatings (often used on cell walls to decrease ^{129}Xe relaxation [41]) [42]; additionally, cell temperature stability and uniformity is often easier to maintain when operating closer to ambient conditions (and for stopped-flow SEOP [20], lower cell temperatures would generally enable faster apparatus cycling and hence greater production of HPXe).

[12] D. Levron et al., Appl. Phys. Lett. **73**, 2668 (1998).

[13] Rb/^{129}Xe SEOP may be impeded by inadvertent simultaneous pumping of the 'red-side' wing of the D_2 line when using broadband sources tuned to the D_1 line [10, 28] ($\Delta\lambda_{D1D2}\approx$15 nm; this effect could play a larger role at high xenon densities, as the D lines are shifted and asymmetrically broadened towards longer wavelengths [10, 43]).

[14] J. Luo et al., Appl. Magn. Reson. **17**, 587 (1999); X. Zhou et al., Chinese Phys. Lett. **21**, 1501 (2004).

[15] B. Driehuys, in: Am. Phys. Soc.: Div. Molec., Atom., Opt. Phys., Charlottesville, VA (2009).

[16] P. Nikolaou et al., J. Magn. Reson. **197**, 249 (2009); N. Whiting, et al., J. Magn. Reson., **208**,

298 (2011).

[17] 1 amagat (amg) = 2.6873×10^{19} cm^3, equal to the density of an ideal gas at 0 °C and 760 Torr.

[18] W. Shao, G. Wang, and E. W. Hughes, Phys. Rev. A **72**, 022713 (2005).

[19] I. Saha et al., Chem. Phys. Lett. **428**, 268 (2006).

[20] M.S. Rosen, et al., Rev. Sci. Instrum. **70**, 1546 (1999).

[21] For 100-1400 Torr Xe, N$_2$ was added to give 2000 Torr total pressure; for 2000 Torr Xe, 600 Torr N$_2$ was added.

[22] B. Chann, et al., Phys. Rev. A 66 033406 (2002).

[23] N. Whiting et al., in: 50th Expl. Nucl. Magn. Reson. Conf., Pacific Grove, CA (2009); M. Barlow et al., in preparation.

[24] T_{OPT} was determined for each Xe density ($\sim$60-65 °C, $\sim$70 °C, and $\sim$85-90 °C for Cs D$_2$, Cs D$_1$, and Rb D$_1$ SEOP, respectively). While we have found an interplay between T_{OPT} and [Xe] using *narrowed* high-power LDAs for Rb [16], here T_{OPT} varied $\lesssim$5 °C using broadband LDAs.

[25] J. Fricke, et al., Phys. Rev. **163**, 45 (1967).

[26] G.D. Domenico and A. Weis, *Wolfram Demonstrations Project* http://demonstrations.wolfram.com/ TransitionStrengthsOfAlkaliMetalAtoms/.

[27] D.A. Steck, http://steck.us/alkalidata, rev. 2.1.2 (2009).

[28] E. Babcock et al., Phys. Rev. Lett. **91**, 123003 (2003).

[29] G.D. Cates et al., Phys. Rev. A **45**, 4631 (1992).

[30] The relative values of [Cs] & [Rb] in Fig. 3 are qualitatively supported by laser-transmittance measurements.

[31] The spin-exchange rate should not depend upon the excitation pathway; thus small differences in γ' for Cs/^{129}Xe D$_1$ & D$_2$ SEOP are not considered significant.

[32] M.P. Augustine, and K.W. Zilm, Mol. Phys. **89**, 737 (1996); Chem. Phys. Lett. **280**, 24 (1997).

[33] C.V. Rice, and D. Raftery, J. Chem. Phys. **117**, 5632 (2002).

[34] In general, ζ has a complex analytical form; In the 'short' molecular lifetime regime [29] and when $P_{AM} \simeq 1$, ζ simplifies to $\Sigma_i f_i \cdot (4I_i + 2)^{-1}$, where f_i is the ith isotope's abundance and I_i is its nuclear spin. In the limits of $P_{AM} \simeq 0$ and $\simeq 1$, ζ_{Rb}=0.179 & 0.095 and ζ_{Cs}=0.172 & 0.0625, respectively. In the 'very short' lifetime regime [29], ζ=1/2 (independent of P_{AM}). In Ref. [18], the short lifetime regime and $P_{AM} \simeq 1$ were assumed. Our experiments are approaching

(or within) the very short lifetime regime.

[35] Temperature dependences of these terms are generally mild (e.g. $\langle\sigma\nu\rangle\propto T^{1/2}$) and are often neglected [18, 29]—as with Γ_{Xe}, because $\Gamma_{Xe}\ll\gamma_{SE}$, $\Delta T/T\ll1$, and its dependence may be nearly flat in our regime (e.g. Ref. [40]). Inclusion of the exponential dependence in Ref. [41] results in only small changes to our γ' values.

[36] S. Kadlecek, L.W. Anderson, and T.G. Walker, Phys. Rev. Lett. **80**, 5512 (1998).

[37] G. Tastevin, J. Low. Temp. Phys. **89**, 669 (1992); W. Heil et al., Phys. Lett. A **201**, 337 (1995).

[38] N. Whiting et al., in: 52nd Expl. Nucl. Magn. Reson. Conf., Pacific Grove, CA (2011).

[39] Z.I. Cleveland, et al., J. Chem. Phys. **124**, 044312 (2006); Stupic, et al., J. Magn. Reson., **208**, 58 (2011).

[40] I.A. Nelson, Ph.D. Thesis, U. Wisconsin (2001).

[41] B. Driehuys, G.D. Cates, and W. Happer, Phys. Rev. Lett. **74**, 4943 (1995).

[42] M. Rosen, personal communication.

[43] M.V. Romalis, et al., Phys. Rev. A **56**, 4569 (1997).

FIG. 1: (color online) Composite figure comprising separate spectra of three high-power broadband LDAs emitting at the Rb D_1, Cs D_2, and Cs D_1 absorption lines, respectively. Laser characteristics (left to right): $\sim$795 nm, $\sim$100 W, $\Delta\lambda_{fwhm}$=2.3 nm; $\sim$852 nm, $\sim$48 W, $\Delta\lambda_{fwhm}$=1.9 nm; $\sim$894 nm, $\sim$46 W, $\Delta\lambda_{fwhm}$=2.9 nm (due to its higher power, the Rb laser's spectrum is normalized to that of the Cs D_2 laser; however, laser powers around $\sim$50 W were used for the experiments reported here).

FIG. 2: (color online) Examples of HP^{129}Xe NMR spectra (at 9.4 T, phase-referenced to an absorptive thermally-polarized ^{129}Xe NMR signal) obtained following ^{129}Xe/Cs D_2 (a) or D_1 (b) SEOP using the same light helicity. Both spectra are frequency-referenced to the chemical shift (δ) of ^{129}Xe gas extrapolated to zero pressure (the asymmetry of the lineshapes results simply from magnetic field inhomogeneities, and is not relevant to the present study). Insets: Corresponding transitions for D_2 and D_1 OP assuming σ^+ CP light (neglecting nuclear contributions; excited-state relaxation is shown as dashed lines—omitted in the D_2 diagram for simplicity).

FIG. 4: (color online) Plots of γ' versus Xe partial pressure for ^{129}Xe/Cs D_1 (red circles), ^{129}Xe/Cs D_2 (blue triangles), and ^{129}Xe/Rb D_1 SEOP (black squares). [Xe]=0.12-2.44 amg. The lines are to guide the eye.

FIG. 5: (color online) Plots of P_{Xe} versus Xe partial pressure following ^{129}Xe/Cs D_1 or ^{129}Xe/Rb D_1 SEOP and transfer to high field. LDA powers: 48 W (Cs) and 52 W (Rb). Estimates for $\langle P_{AM} \rangle$ are inferred from P_{Xe}, γ_{SE}, and Γ_{Xe} values and Eq. (2).

FIG. 3: (color online) (a) Selected P_{Xe} build-up curves obtained during ^{129}Xe/Cs or ^{129}Xe/Rb SEOP (2000 Torr Xe, 600 Torr N_2). Cell temperatures (measured from oven air exhaust) and nominal laser conditions: 70 °C & 46 W ($\Delta\lambda_{fwhm}$=2.9 nm) for Cs D_1; 60 °C & 40 W ($\Delta\lambda_{fwhm}$=1.9 nm) for Cs D_2; and 80 °C & 53 W ($\Delta\lambda_{fwhm}$=2.1 nm) for Rb D_1. (b,c) Plots of Γ versus [Rb] (b) or [Cs] (c) (estimated from vapor-pressure curves [27]) for SEOP with various Xe densities; (c) contains Cs D_1 and D_2 SEOP results. Lines are fits to the aggregate data (see text).
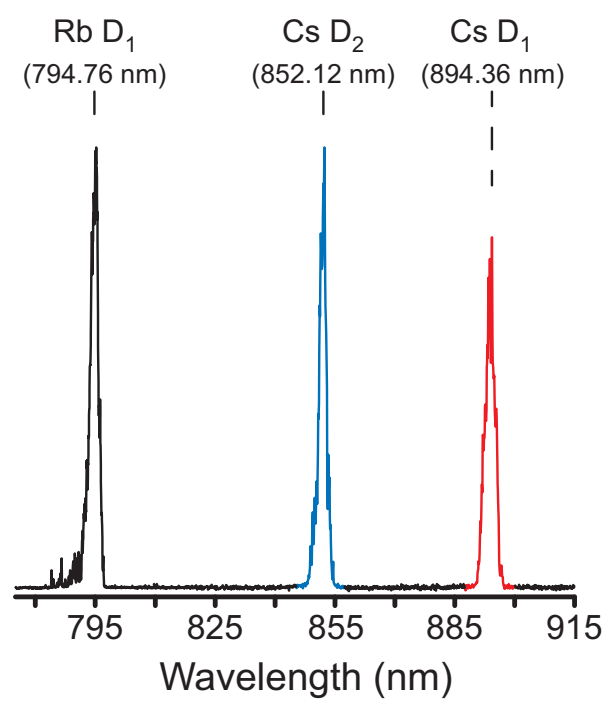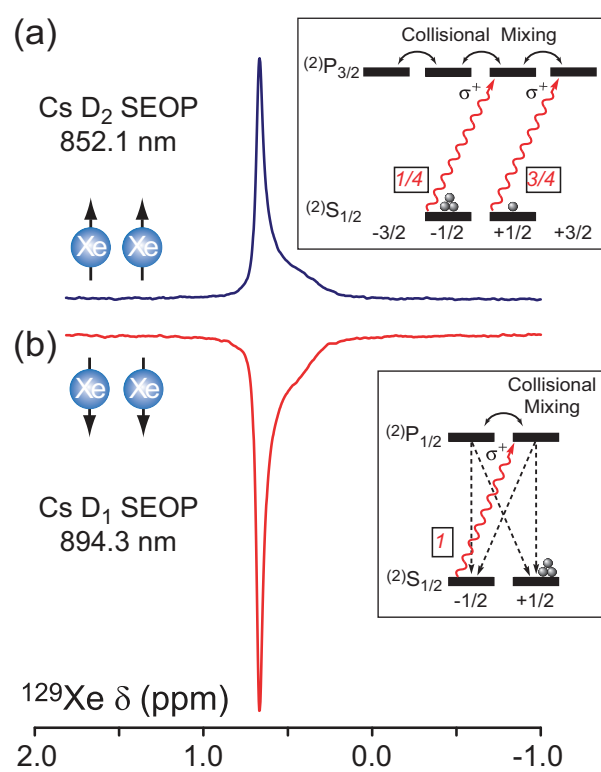
Rb D$_1$
(794.76 nm)

Cs D$_2$
(852.12 nm)

Cs D$_1$
(894.36 nm)

795   825   855   885   915

Wavelength (nm)

Figure 1   LY12443A   28Apr2011

(a)

Cs D$_2$ SEOP
852.1 nm

Collisional Mixing

$^{(2)}$P$_{3/2}$

σ^+ σ^+

1/4   3/4

$^{(2)}$S$_{1/2}$
-3/2 -1/2 +1/2 +3/2

(b)

Cs D$_1$ SEOP
894.3 nm

Collisional
Mixing

$^{(2)}$P$_{1/2}$

σ^+

1

$^{(2)}$S$_{1/2}$
-1/2   +1/2

^{129}Xe δ (ppm)

2.0   1.0   0.0   -1.0

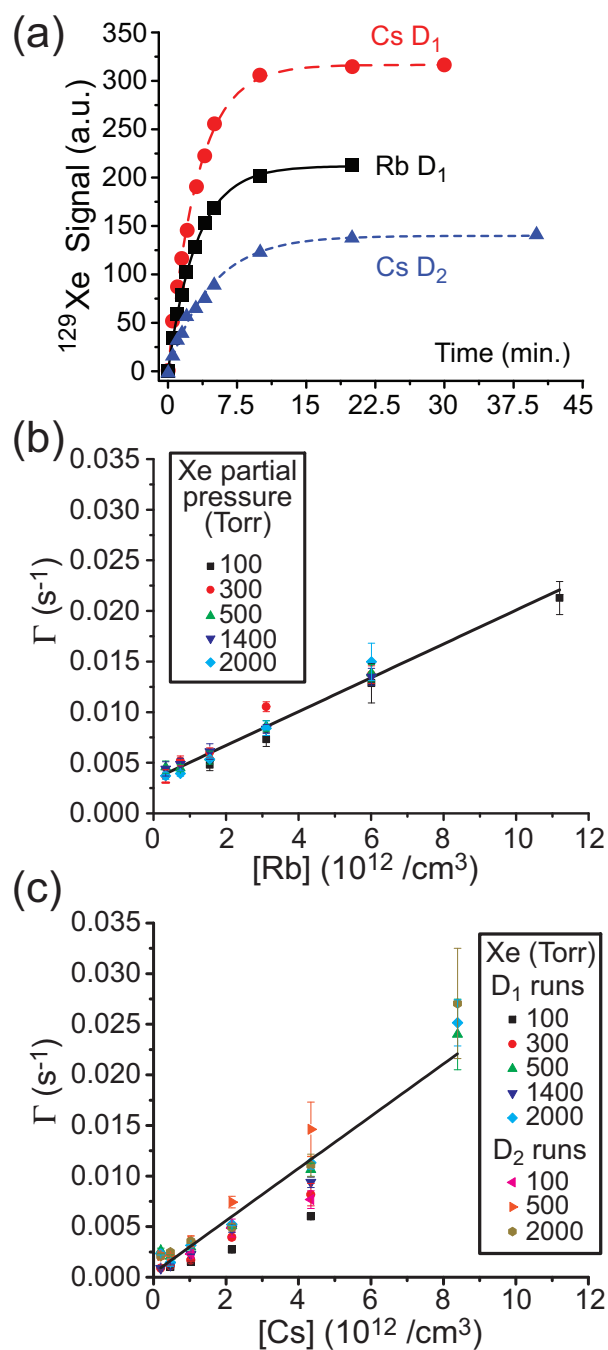Figure 2   LY12443A   28Apr2011

(a)

(b)

(c)

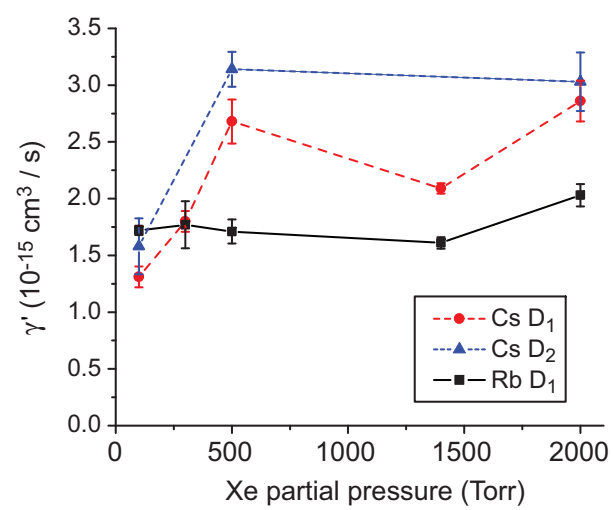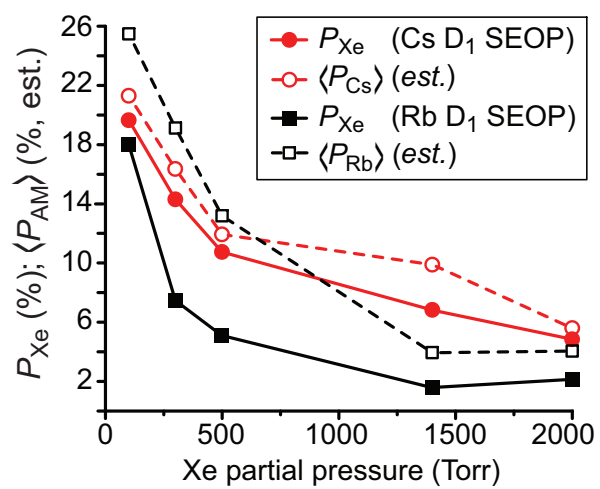Figure 3   LY12443A   28Apr2011

Figure 4   LY12443A   28Apr2011

Figure 5   LY12443A   28Apr2011